Electronic conduction above 4 K of slightly reduced oxygen-deficient rutile TiO_{2-x}

Eiichi Yagi
The Institute of Physical and Chemical Research (RIKEN), Wako-shi, Saitama 351-01, Japan

Ryukiti R. Hasiguti
Faculty of Engineering, The University of Tokyo, Hongo, Bunkyo-ku, Tokyo 113, Japan

Masakazu Aono
The Institute of Physical and Chemical Research (RIKEN), Wako-shi, Saitama 351-01, Japan
(Received 6 July 1995; revised manuscript received 6 May 1996)

Based on electrical resistivity and Hall-coefficient measurements from 2 to 370 K on slightly reduced semiconductive rutile single crystals with various oxygen deficiencies O_d from 3.7×10^{18} to $1.3\times10^{19}/cm^3$, electronic conduction above 4 K is discussed in terms of two conduction bands separated by 0.03–0.05 eV. In this range of O_d, defects are mostly Ti interstitial ions. Ionization of Ti interstitial donors takes place above about 4 K. The ionization energy E_2 depends on the donor concentration N_D and decreases with increasing N_D for $O_d<1\times10^{19}/cm^3$. The density of states effective mass m_d^{**} of the lower conduction band is estimated to be $(7-8)m_e$ (m_e is the free electron mass). The anisotropy of the effective mass is also estimated to be roughly $m_c^{**}\cong(2-4)m_e$ and $m_a^{**}\cong(10-16)m_e$ in the **c** and **a** directions, respectively. The mobility above 50 K of the lower conduction band electrons is discussed. [S0163-1829(96)06235-2]

I. INTRODUCTION

Rutile (TiO_2) has a tetragonal crystal structure with lattice parameters $a=4.594$ Å and $c=2.959$ Å, and, therefore, has a large anisotropy in various properties.[1] At the stoichiometric composition it is an insulator with an energy band gap of about 3 eV. Upon slight reduction it becomes an n-type semiconductor, because nonstoichiometric defects that are introduced by the reduction treatment act as donor centers. Therefore, its electronic conduction is closely related to defect structures.

Electronic conduction below 3 K is well explained in terms of hopping of electrons from lattice defect to lattice defect (donor to donor) in a process similar to the impurity conduction that is observed in elemental semiconductors such as Si and Ge.[2–5] On the other hand, for the interpretation of electronic conduction above 4 K, various mechanisms have been proposed involving either small polaron[6] or standard band conduction in one[7] or two[3,8] bands, and a variety of values for the conduction electron effective mass have been reported.

Defect structures have been extensively studied by various experimental methods, and various types of defects have been reported. The defect structure varies with oxygen deficiency O_d, but the question of which type of defect is dominant in which region of O_d is still under discussion (Ref. 5 and references therein). In order to identify defects we have performed experiments by electron paramagnetic resonance (EPR),[9–11] transmission electron microscopy,[12] and channeling methods,[13] and have shown conclusively that the dominant defects are Ti interstitials in the region of O_d investigated, i.e., $3.7\times10^{18}<O_d<1.3\times10^{19}/cm^3$ (from $TiO_{1.9996}$ to $TiO_{1.9999}$).

In the present paper, electronic conduction above 4 K is discussed in connection with defect structures on the basis of the results of measurements of electrical resistivities ρ, Hall coefficients R_H, and their anisotropies. Electronic conduction below 3 K has already been discussed in a previous paper.[5]

II. EXPERIMENTAL PROCEDURE

Plate-shaped parallelepiped specimens of size about $12\times5\times0.8$ mm^3 were cut from two single-crystal boules A and B of nominal purity 99.99%, which differ slightly in actual purity. For the anisotropy study specimens having the following two orientations were prepared from the same boule: one with the longest edge parallel to the **c** axis and the largest face perpendicular to the **a** axis (ca specimen), and another with the longest edge parallel to the **a** axis and the largest face perpendicular to the **c** axis (ac specimen) [Figs. 1(a) and 1(b)].

These were slightly reduced in vacuum to obtain the desired O_d, then cut into the so-called bridge shape with six side arms for attaching potential leads and Hall leads on both sides of the stem crystal, as shown in Fig. 1(c). The experimental method for the vacuum reduction has been described in detail in a previous paper.[5] Copper lead wires of diameter 0.1 mm were soldered to the arms with indium. It was confirmed that Ohmic contact was achieved. Electrical resistivities and Hall coefficients were measured from 2 to 370 K by the conventional 6-terminal dc technique. In the electrical measurements current was supplied in the direction of the longest edge, i.e., the **c** axis for ca specimens and the **a** axis for ac specimens. The resistivities thus measured are denoted by ρ_c and ρ_a, respectively. For R_H measurement, a magnetic field **H** between 2000 and 3000 G was applied in the direction perpendicular to the largest face, i.e., **H**$\|$**a** for ca specimens and **H**$\|$**c** for ac specimens. The Hall coefficients thus obtained are denoted by $R_{H,a}$ and $R_{H,c}$, respec-

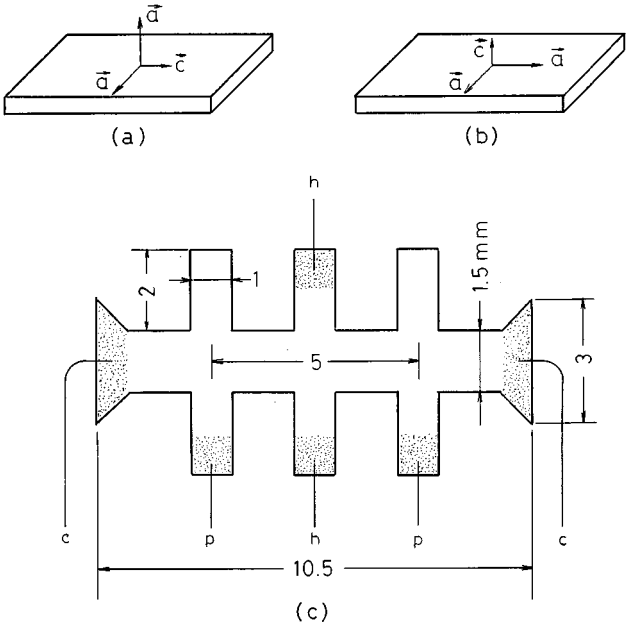

FIG. 1. Crystallographic orientations of (a) *ca* specimens and (b) *ac* specimens, and (c) the dimensions of the bridge-shaped specimen. The thickness of the specimens is about 0.8 mm. **c**, current lead; **p**, potential lead; and **h**, Hall lead.

tively. In the ρ measurements two readings were taken with opposite directions of specimen current to eliminate thermal emf, and their average was used as the value of resistivity. In the R_H measurements two readings were taken with opposite directions of magnetic field for each direction of specimen current. The resistivities and the Hall coefficients were still reproducible in measurements made after the specimens had been kept at room temperature for six months.

III. EXPERIMENTAL RESULTS

Reduction temperatures T_R and oxygen deficiencies O_d of the specimens are listed in Table I. Figures 2 and 3 show results of ρ_c and $R_{H,a}$ measurements for the *A*-boule *ca* specimens with various values of O_d up to $1.3\times10^{19}/\mathrm{cm}^3$. (Figure 2 has already been shown in a previous paper.[5]) The R_H curves exhibit two maxima or shoulders at about 3 and 110 K. Below 3 K, $R_{H,a}$ decreases with decreasing tempera-

TABLE I. List of specimens. Oxygen deficiency O_d, reduction temperature T_R, and resistivity at 300 K, $\rho_{300\ \mathrm{K}}$.

Boule	Specimen No.	O_d (cm^{-3})	T_R (K)	$\rho_{300\ \mathrm{K}}$ (Ω cm)
	*A*1	3.7×10^{18}	1273	2.48
	*A*2	4.5	1273	1.52
	*A*3	5.0	1373	1.46
A	*A*4	5.5	1373	1.35
	*A*5	8.5	1273	0.88
	*A*6	10	1273	1.14
	*A*7	13	1273	1.04
	B1ca	7.4	1273	0.81
B	B1ac	7.4	1273	3.04

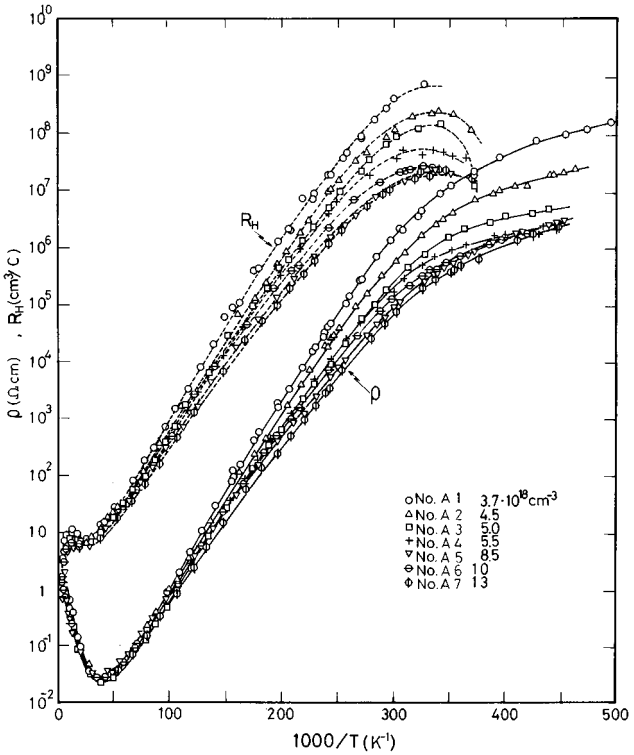

FIG. 2. Electrical resistivities ρ and Hall coefficients R_H measured for *ca* specimens with various oxygen deficiencies O_d from 3.7×10^{18} to $1.3\times10^{19}/\mathrm{cm}^3$ as a function of reciprocal temperature $1/T$.

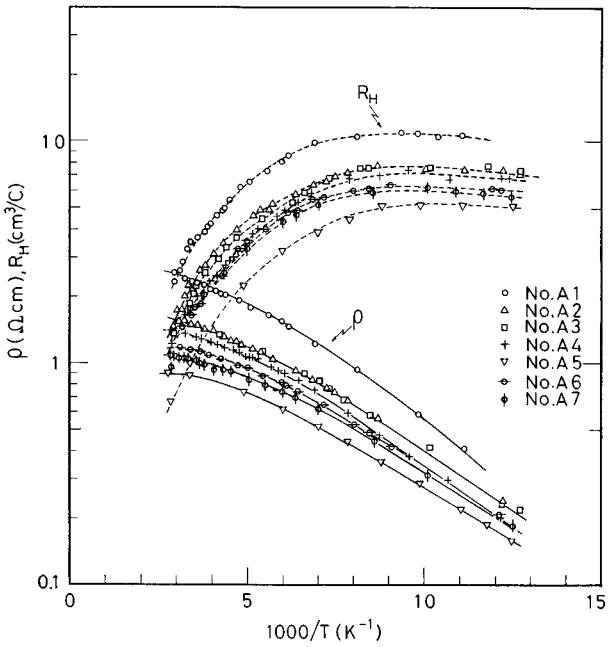

FIG. 3. Electrical resistivities ρ and Hall coefficients R_H measured at temperatures higher than 77 K for the *ca* specimens with various oxygen deficiencies O_d from 3.7×10^{18} to $1.3\times10^{19}/\mathrm{cm}^3$ as a function of reciprocal temperature $1/T$.

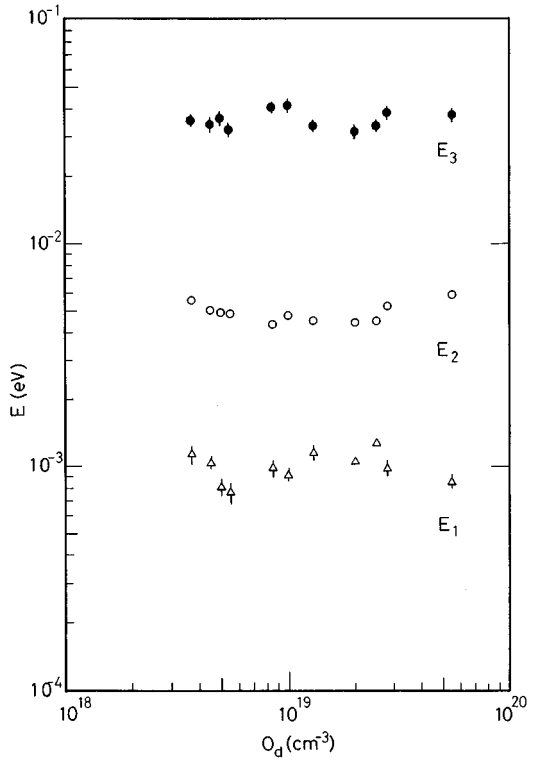

FIG. 4. Activation energies E_1, E_2, and E_3 as a function of oxygen deficiency O_d. The results previously obtained for $O_d > 1.3\times10^{19}/cm^3$ are also included. The error bars of the values of E_2 are within the size of the symbols (open circles).

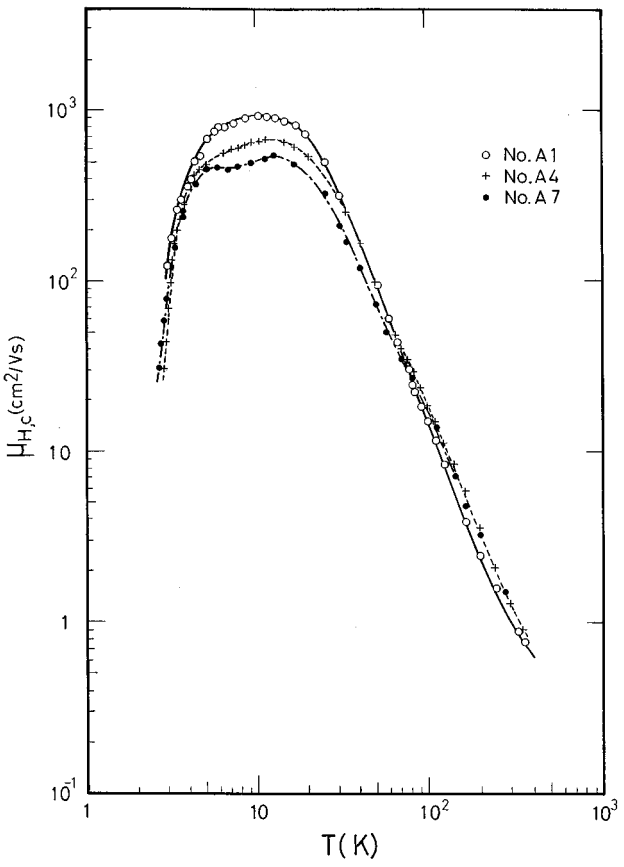

FIG. 5. Hall mobilities μ_H for three specimens.

ture, while ρ_c increases with a very small activation energy. Between about 4 and 20 K, both $R_{H,a}$ and ρ_c decrease with increasing temperature and are approximated in the form of $C\exp(E/kT)$. Above 30 K, ρ_c begins to increase. Three temperature regions are apparent, as distinguished by distinctive features of the $R_{H,a}$ versus $1/T$ curves, below 3 K, from 4 to 40 K, and above 110 K. Activation energies obtained in each temperature region are denoted by E_1, E_2, and E_3, respectively. E_1 was determined from a ρ versus $1/T$ curve below about 3 K under the approximation $\rho=\rho_0\exp(E/kT)$. E_2 was deduced from the slope of a $\log_{10}(R_{H,a}T^{3/2})$ versus $1/T$ curve between 5.5 and 12 K by assuming $R_{H,a}=1/nec$, as described in Sec. IV A. This temperature range was chosen so that the slopes of these curves are not affected by the presence of the maxima or shoulders around 3 and 110 K [cf. Fig. 9, where $n/T^{3/2}\propto(R_{H,a}T^{3/2})^{-1}$]. E_3 was obtained from the slope of a $\log_{10}(R_{H,a})$ versus $1/T$ curve between 210 and 250 K. E_1, E_2, and E_3 are plotted in Fig. 4 as a function of O_d together with previously reported results for $O_d > 1.3\times10^{19}/cm^3$. E_2 decreases with increasing O_d in the region $O_d < 10^{19}/cm^3$, but increases in the region $O_d > 10^{19}/cm^3$. E_3 is approximately independent of O_d.

Figure 5 shows Hall mobilities $\mu_{H,c}$ $(=R_{H,a}/\rho_c)$ for three ca specimens as typical examples. They exhibit a maximum around 15 K. Above 30 K, their temperature dependence can be approximated by $T^{-(2.5-3.0)}$. The maximum value around 15 K decreases with increasing O_d in the region $O_d < 10^{19}/cm^3$.

To investigate the anisotropy in the conduction process, ρ and R_H were measured for the B-boule ca and ac specimens, $B1ca$ and $B1ac$, which had been reduced in the same ampoule to have the same O_d. The values of $(\rho_c, R_{H,a})$ and $(\rho_a, R_{H,c})$ are shown in Figs. 6 and 7, and the anisotropy ratios ρ_a/ρ_c and $R_{H,c}/R_{H,a}$ are shown in Fig. 8. Below 40 K, R_H is negligibly dependent on the specimen orientation, whereas ρ is orientation dependent, with ρ_a larger than ρ_c by a factor of 2–3, i.e., $\rho_a/\rho_c=2$–3. Becker and Hosler also reported $\rho_a/\rho_c=2$ (Ref. 8). Above 40 K, R_H shows orientation dependence. The activation energy of E_3 obtained from the $R_{H,c}$ curve is about 0.08 eV, which is two to three times as large as that obtained from the $R_{H,a}$ curve of the ca specimen. It is to be noted that ρ_a shows a maximum at about 300 K and decreases with increasing temperature above 300 K. On the other hand, ρ_c shows no such maximum up to 370 K, which is the highest temperature covered in the present experiment and continues to increase very slowly above 300 K.

IV. DISCUSSION

From the point of view of chemical bonding rutile is regarded as intermediate between ionicity and covalency.[1] In polar crystals the interaction of conduction electrons with lattice polarization is important. Therefore, in reduced rutile the polaron effect on electronic conduction must be taken into account. For a polaron there are two limiting situations, i.e., the large and small polaron limits, depending on its size r_f, which is a measure of the extent of lattice distortion induced by excess electrons.[14]

If r_f is larger than a lattice constant, the large polaron

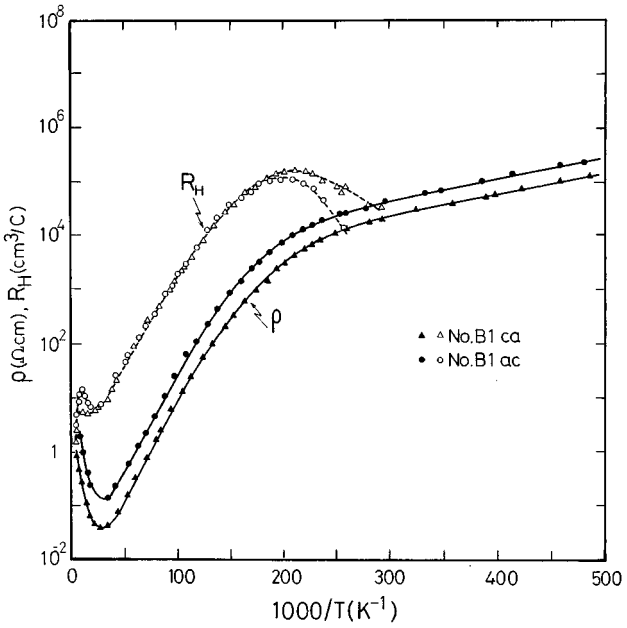

FIG. 6. Electrical resistivities ρ and Hall coefficients R_H measured for specimens $B1ca$ and $B1ac$ as a function of reciprocal temperature $1/T$.

model can be applied. In the case that the electron-lattice interaction measured by the coupling constant α is small, the ionic polarization field, which is determined by the dynamical properties of the lattice, adiabatically follows the slow translational motion of the excess electron. For large α (strong coupling), the electron becomes self-trapped in a bound state of its own displacement field. In both cases the conduction process can be interpreted in terms of the standard band model with a modified effective mass.[14]

If r_f is smaller than a lattice constant, the small polaron model can be applied. In this case the coupling constant is large and the excess electron is strongly localized around a single lattice ion. At low temperatures, narrowing of the conduction band due to the electron-lattice interaction must be considered and the bandwidth is temperature dependent. At high temperatures of the order of $\hbar\omega_0/(2k)$ (ω_0 is the frequency of the longitudinal lattice polarization field), the bandwidth becomes so narrow that the band picture breaks down. The electron motion between such small polaron states proceeds via a phonon-activated hopping process, and in this regime, drift mobility increases exponentially with temperature.[14]

According to the polaron theory, the polaron effective mass m^{**} can be estimated if the electron-lattice coupling constant and the rigid lattice mass m^* are known. The latter accounts for the effect of the periodic lattice on the electron motion when ions are fixed at their equilibrium positions. On the basis of the investigations on the width of the conduction band by various authors, Bogomolov, Kudinov, and Firsov suggested that m^* was on the order of $(3–5)m_e$ (m_e is the free-electron mass), neglecting the crystal anisotropy.[6]

The characteristic length u^{-1}, which has a value of nearly the same order as r_f, is given by $u^{-1}=(2m^*\omega_0/\hbar)^{-1/2}$ (Ref. 14). If, in a rutile crystal, the maximum longitudinal mode frequency $\omega_0=1.5\times10^{14}$ s^{-1} (Ref. 15) and the rigid lattice mass given above are used, it follows that $u^{-1}=2.8–3.6$ Å. Considering that m^* was estimated by neglecting the anisotropy, it is possible that the criterion for the large polaron model is satisfied in the **c** direction, i.e., $r_f>c$. It might be said that r_f lies in a region intermediate between the small polaron and large polaron models.

A. Effective mass

Both models allow consideration of the band conduction process at low temperatures. Therefore, as described below, the density of states effective mass m_d^{**} of the conduction band can be estimated from R_H data below about 20 K. In this temperature region the ionization of donor centers takes place. When only one kind of donor center is present, the number of electrons in the conduction band, n, is given by the following equation at low temperatures where the condition $N_D>N_A\gg n$ can be satisfied:

$$n=\frac{N_D-N_A}{N_A}\frac{N_c}{2}\left(\frac{m_d^{**}}{m_e}\right)^{3/2}\exp\left(-\frac{E_2}{kT}\right),$$

$$N_c=2(2\pi m_e kT/h^2)^{3/2}. \tag{1}$$

Here N_D and N_A represent the donor and acceptor concentrations, respectively. According to the small polaron model, the effective mass is temperature dependent in the form

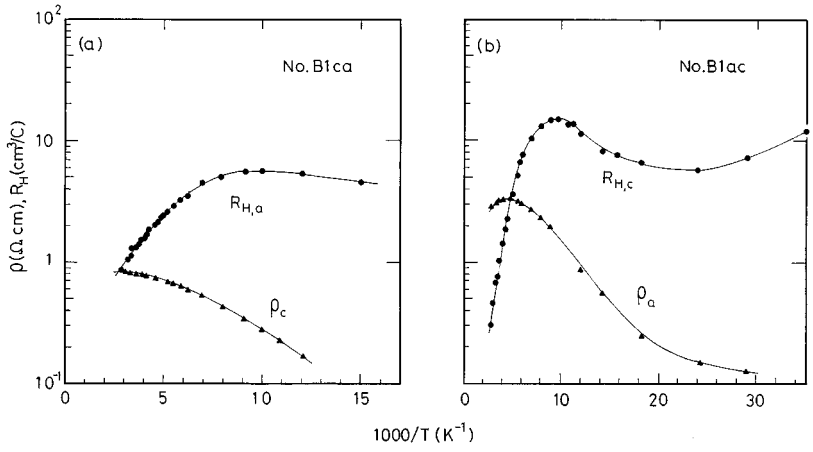

FIG. 7. Electrical resistivities ρ and Hall coefficients R_H measured at temperatures higher than 77 K for specimens (a) $B1ca$ and (b) $B1ac$ as a function of reciprocal temperature $1/T$.

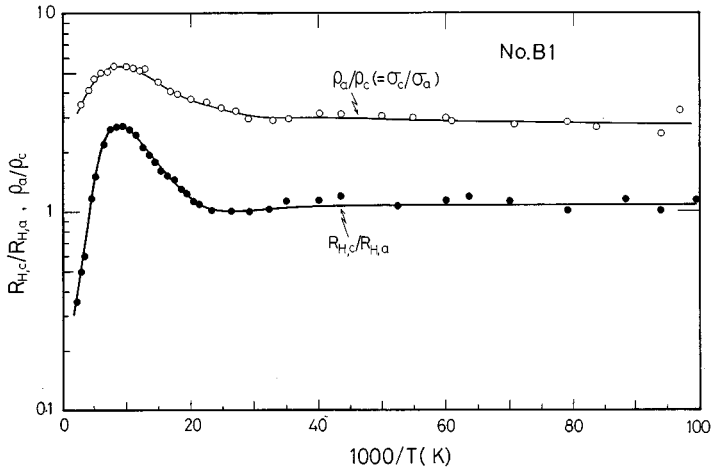

FIG. 8. Anisotropy ratios of electrical resistivities ρ_a/ρ_c, and Hall coefficients $R_{H,c}/R_{H,a}$ for specimens $B1ca$ and $B1ac$ as a function of reciprocal temperature $1/T$.

$$m_d^{**}=m_d^{*}\exp\left(\frac{S_m(T)}{\kappa_{\rm op}^2}\right), \tag{2}$$

through $S_m(T)$, which contains a factor $\coth(\hbar\omega_0/kT)$.[16] $\kappa_{\rm op}$ represents the optical dielectric constant. In the low-temperature region where $(\hbar\omega_0/kT)>2$, $\coth(\hbar\omega_0/kT)$ becomes nearly temperature independent. Even if the lowest longitudinal mode frequency 7×10^{13} s^{-1} is taken for ω_0 (Ref. 15), m_d^{**} can be considered to be temperature independent below 267 K. Therefore, in either the large or the small polaron model the effective mass m_d^{**} can be estimated from Eq. (1) by considering m_d^{**} to be constant. In the present paper, as described later, the conductivity is interpreted on the basis of the two-conduction-band model. As the lower conduction band provides the basic contribution to the electronic conduction below 100 K, the effective mass discussed here is that related to the lower conduction band. The carrier concentration n can be estimated from the Hall coefficient R_H using the equation

$$R_H=\left(\frac{\mu_H}{\mu}\right)\left(\frac{1}{nec}\right). \tag{3}$$

In the usual band model, the ratio of Hall to drift mobilities μ_H/μ is constant and nearly equal to unity. In the small polaron band regime, this ratio is crystal structure dependent. If the structure has a square lattice in the plane perpendicular to magnetic field **H**, the ratio is unity.[17] This is the case for $R_{H,c}$ in rutile. As shown in Fig. 8, R_H is isotropic below 40 K. Therefore, the ratio can be considered to be nearly unity in both large and small polaron models. Hence we assume $\mu_H/\mu=1$ below 40 K. From Eq. (1), it follows that

$$\left(\frac{n}{T^{3/2}}\right)_{1/T\to0}=\frac{N_D-N_A}{N_A}\left(\frac{2\pi m_e k}{h^2}\right)^{3/2}\left(\frac{m_d^{**}}{m_e}\right)^{3/2}. \tag{4}$$

If N_D and N_A are known, m_d^{**}/m_e can be estimated from the extrapolation of the $\ln(n/T^{3/2})$ versus $1/T$ curve below 20 K to $1/T\to0$. Since the defects are mostly Ti interstitial donors in the specimens with O_d less than $10^{19}/\text{cm}^3$, N_D is estimated from the relation $N_D\cong\frac{1}{2}O_d$. For N_A we have no definite information. N_A is considered to depend on the impurity concentration and, in some cases, on the oxygen deficiency. It may be assumed, however, that it is nearly constant within a narrow range of oxygen deficiency. Under this assumption, the value of (m_d^{**}/m_e) was estimated from the experimental data for the three specimens $A2$, $A3$, and $A4$ whose oxygen deficiencies fall in the narrow range of $(4.5\text{–}5.5)\times10^{18}O_d/\text{cm}^3$. The $\ln(n/T^{3/2})$ vs $1/T$ curves for the three specimens are shown in Fig. 9. In the temperature range from 5 to 12 K the curves agree well with Eq. (1), and the curves in this range are extrapolated to $1/T\to0$. Taking account of the scattering of the data points, the ranges of the extrapolated values of $(n/T^{3/2})_{1/T\to0}$ and the values of E_2 are listed in Table II. The value of (m_d^{**}/m_e) thus estimated ranges from 2 to 13. It follows that

$$m_d^{**}=(7-8)m_e. \tag{5}$$

In terms of a simple many-valley conduction-band model, m_d^{**} is expressed as

$$m_d^{**}=N_V^{2/3}(m_1^{**}m_2^{**}m_3^{**})^{1/3}, \tag{6}$$

where N_V is the number of valleys, and m_1^{**}, m_2^{**}, and m_3^{**} are the mass parameters along the three principal axes of the ellipsoidal energy minima.[18] Measurements of the piezoresistivity of reduced rutile above 78 K suggest that the minimum of the conduction band is located on the k_z axis in **k** space and that the band is not degenerate.[19] From the crystal symmetry the energy surface consists of one or two ellipsoids of revolution with respect to the k_z axis. Energy ellipsoids have three principal axes along **a**, **a**, and **c** crystal axes and have effective masses m_a^{**}, m_a^{**}, and m_c^{**} associated with each axis, i.e.,

$$m_d^{**}=N_V^{2/3}(m_a^{**}m_a^{**}m_c^{**})^{1/3}. \tag{7}$$

The values of m_a^{**} and m_c^{**} are estimated from the anisotropy in mobility at low temperatures. For the ellipsoidal energy surface model under consideration, the conductivities σ_a, σ_c and their anisotropy ratio σ_c/σ_a, and Hall coefficients $R_{H,c}$, $R_{H,a}$ and their anisotropy ratio $R_{H,c}/R_{H,a}$ are given by the following equations:[20]

$$\sigma_a=n\frac{e^2}{m_a^{**}}\langle\tau_a\rangle,\quad \sigma_c=n\frac{e^2}{m_c^{**}}\langle\tau_c\rangle,\quad \frac{\sigma_c}{\sigma_a}=\frac{m_a^{**}}{m_c^{**}}\frac{\langle\tau_c\rangle}{\langle\tau_a\rangle}, \tag{8}$$

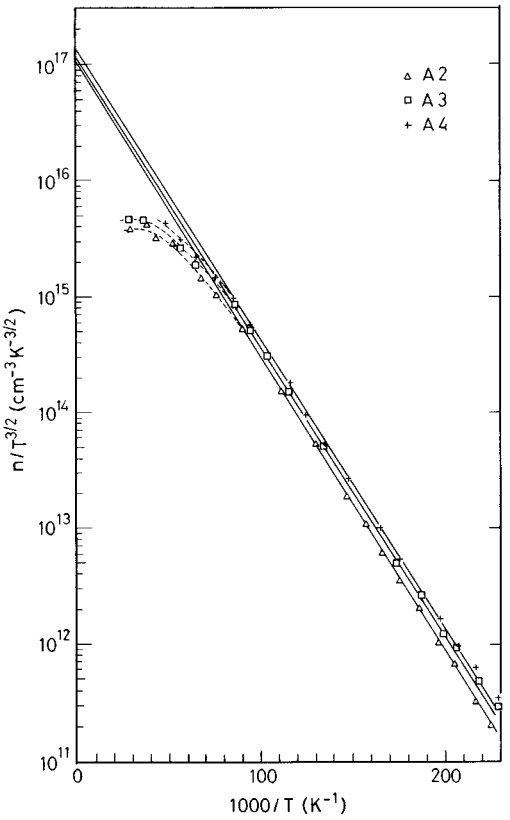

FIG. 9. $n/T^{3/2}$ values for specimens $A2$, $A3$, and $A4$ as a function of reciprocal temperature $1/T$.

$$R_{H,c}=\frac{1}{nec}\frac{\langle\tau_a^2\rangle}{\langle\tau_a\rangle^2},\quad R_{H,a}=\frac{1}{nec}\frac{\langle\tau_a\tau_c\rangle}{\langle\tau_a\rangle\langle\tau_c\rangle},$$

TABLE II. $(n/T^{3/2})_{1/T\to 0}$ (n is the carrier concentration), donor concentration N_D, and ionization energy E_2 for specimens $A2$, $A3$, and $A4$.

Specimen No.	$(n/T^{3/2})_{1/T\to 0}$ ($cm^{-3}K^{-3/2}$)	N_D (cm^{-3})	E_2 (eV)
$A2$	$(1.04–1.10)\times10^{17}$	2.25×10^{18}	$(5.00–5.10)\times10^{-3}$
$A3$	1.15–1.22	2.50	4.88–5.00
$A4$	1.32–1.40	2.75	4.85–4.96

$$\frac{R_{H,c}}{R_{H,a}}=\frac{\langle\tau_a^2\rangle\langle\tau_c\rangle}{\langle\tau_a\rangle\langle\tau_a\tau_c\rangle}.$$

The assumption that $R_{H,c}=1/nec$ corresponds to the relation $\langle\tau_a^2\rangle/\langle\tau_a\rangle^2=1$. If $\tau_a/\tau_c=$const, it follows that $R_{H,c}/R_{H,a}=1$ and $\sigma_c/\sigma_a=$const. This is the case below 40 K, as shown in Fig. 8. Below 30 K, the Hall mobility and, therefore, the drift mobility, are oxygen deficiency dependent (Fig. 5). In this temperature region, scattering by ionized centers is important. For the anisotropy in the conductivity due to this scattering mechanism, theoretical calculations have been performed by Samoilovich *et al.*[21,22] and Korenblit.[23] Figure 10 shows the relationship among m_a^{**}/m_c^{**}, τ_a/τ_c, and σ_c/σ_a, which was obtained from the results of Korenblit's calculation[23] and Eq. (8). The experimental result $\rho_a/\rho_c=\sigma_c/\sigma_a=2-3$ indicates that the energy surface is oblate ellipsoidal with an effective-mass anisotropy $p=m_a^{**}/m_c^{**}=4-10$.

In the case of an oblate ellipsoidal energy surface, the mobility in the **c** direction due to scattering by ionized centers $\mu_{i,c}$ is given by

$$\mu_{i,c}=\frac{e}{m_c^{**}}\langle\tau_c\rangle\cong A\frac{(1-p)^2(1+\frac{4}{25}p)}{\{(p-1)+\frac{1}{2}\sqrt{(p-1)/p}\,\ln[(\sqrt{p}-\sqrt{p-1})/(\sqrt{p}+\sqrt{p-1})]\}\ln[(24m_c^{**}kT/\hbar^2)\kappa_{\rm st}kT/4\pi e^2n']},$$

$$A=\frac{2^{9/2}\kappa_{\rm st}^2m_c^{**1/2}(kT)^{3/2}}{3\pi^{3/2}N_Ie^3m_a^{**}},$$

$$n'=n+(n+N_A)\left(1-\frac{n+N_A}{N_D}\right),\tag{9}$$

where N_I is the concentration of ionized centers and $\kappa_{\rm st}$ is the static dielectric constant.[21,23] As seen from Fig. 5, the mobility has a maximum around 15 K, which results from the competition between scattering by ionized centers and by phonons. When both contributions to mobility become equal, the observed mobility $\mu_{\rm expt}$ exhibits a maximum and is expected to have the value $\frac{1}{2}\mu_{i,c}$ because $(1/\mu)=(1/\mu_{i,c})+(1/\mu_{\rm phon})$. Therefore, $\mu_{i,c}$ is expected to take the value $2\mu_{\rm expt}$ around 15 K. For specimen $A4$, which has $N_D=2.75\times10^{18}/cm^3$ and $N_A=0.67\times10^{18}/cm^3$, the mobility $\mu_{i,c}$ at 15 K was calculated for various combinations of p ($4\leqslant p\leqslant10$) and m_c^{**}/m_e. In this calculation N_I was taken to be equal to $2N_A$, because N_A donors become ionized due to the trapping of N_A electrons by N_A acceptors. The magnitude of N_A was estimated from Eq. (1) using $m_d^{**}=7m_e$. The static dielectric constants $\kappa_{\rm st}$ are 89 in the **a** direction and 173 in the **c** direction.[24] In the present calculation the average value for a powder sample, 117, was used. The results are shown in Fig. 11. The experimental value $\mu_{\rm expt}$ at 15 K is about 650 $cm^2/V\,s$. Taking account of uncertainty in the value used for $\kappa_{\rm st}$ in the calculation, the effective mass m_c^{**} is roughly estimated to be $(2–4)m_e$ so that $\mu_{i,c}$ has a

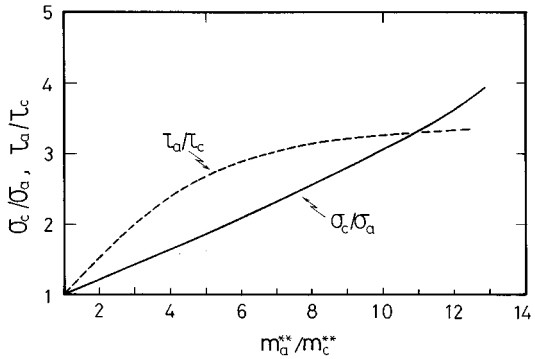

FIG. 10. The relationship among conductivity anisotropy σ_c/σ_a, effective-mass anisotropy m_a^{**}/m_c^{**}, and relaxation time anisotropy τ_a/τ_c in the case of ionized center scattering.

value between μ_{expt} and $2\mu_{\text{expt}}$.

The value of m_c^{**} can also be estimated from Eq. (7) with the condition $4 \leqslant p \leqslant 10$. Figure 12 shows the obtained relationship among m_c^{**}, m_a^{**}, and p for $m_d^{**}=(7-8)m_e$ and $N_V=1$ or 2. The value of m_c^{**} falls in the region $(1-4)m_e$, which is in good agreement with the value estimated above. Better agreement is obtained for $N_V=1$, i.e., a single ellipsoid. For $N_V=1$, $m_a^{**} \cong (10-16)m_e$. From these analyses it follows that

$$m_d^{**} \cong (7-8)m_e, \quad m_c^{**} \cong (2-4)m_e,$$

$$m_a^{**} \cong (10-16)m_e. \tag{10}$$

For the density of states effective mass various values have been reported based on measurements of properties such as thermoelectric power Q and specific heat. The values vary in a very wide range from $2m_e$ to $190m_e$. From measurements of Q in the temperature region from 100 to 300 K, Thurber and Mante,[25] Acket and Volger,[7] and Cristea and Babes[26] derived $(20-35)m_e$ at room temperature, $(5-13)m_e$ at 300 K and $(2-8)m_e$ at 150 K, respectively. Frederikse[27] derived $(12-32)m_e$ from similar measurements above 300 K.

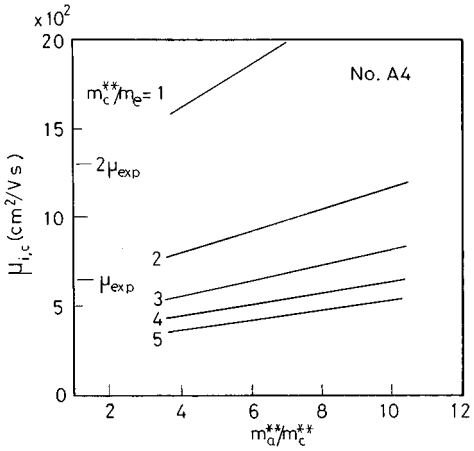

FIG. 11. Mobilities in the **c** direction $\mu_{i,c}$ calculated for specimen $A4$ using Eq. (9). μ_{expt} represents the experimental value of the mobility at 15 K.

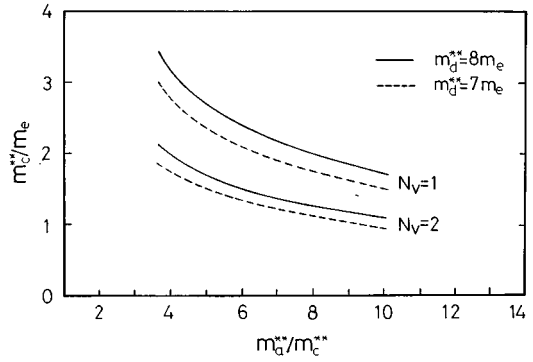

FIG. 12. Effective masses m_c^{**} calculated from Eq. (7) for various values of effective-mass anisotropy m_a^{**}/m_c^{**}.

These values were estimated based on the one-conduction-band model. Baumard and Gevais[28] obtained $(8-10)m_e$ from the study of infrared reflectivity at room temperature for more heavily reduced specimens than those used in most experiments. Pascual, Camassel and Mathieu[29] estimated the lower limit of the effective mass to be $8m_e$ based on optical absorption experiments from 1.6 to 300 K. On the other hand Sandin and Keeson[30] derived the very large value of $190m_e$ from measurements of specific heat between 0.3 and 20 K. DeFord and Johnson[31] reported $12.5m_e$ as a rough estimate based on a study of ρ and R_H for Nb- and Nb+H-doped rutile specimens from 6 to 40 K. This value is of the same order of magnitude as the present result.

In the following section, the experimental value of the effective mass will be compared with the values calculated from polaron theories. In the large polaron model the coupling constant α is given by[32]

$$\alpha = \frac{1}{2}\left(\frac{1}{\kappa_{\text{op}}} - \frac{1}{\kappa_{\text{st}}}\right)\left(\frac{e^2 u}{\hbar\omega_0}\right). \tag{11}$$

Substituting $\omega_0=1.5\times10^{14}$ s^{-1}, $\kappa_{\text{op}} \cong 7$ (Ref. 27), and $\kappa_{\text{st}} \cong 117$ into Eq. (11), it follows that $\alpha=2.7-3.5$. This range of values of α is typical for the case of intermediate coupling. Lee, Low, and Pines determined that for the intermediate coupling case ($\alpha \leqslant 6$) in the large polaron model, the conductivity effective mass m^{**} is given by[33]

$$m^{**} = m^*(1+\alpha/6). \tag{12}$$

The assumption that $m^*=(3-5)m_e$ thus leads to $m^{**}=(4-8)m_e$, whereas from other relations given by Schultz[34] [$m^{**}=1.89m^*$ ($\alpha=3$) and $m^{**}=3.89m^*$ ($\alpha=5$)], it follows that $m^{**}=(6-20)m_e$.

On the other hand, the small polaron effective mass is nearly temperature independent below $T<\hbar\omega_0/(2k)$ and approximated by

$$m^{**} \cong m^* \exp\left(\frac{S_m(T=0)}{\kappa_{\text{op}}^2}\right). \tag{13}$$

The factor $S_m(T=0)$ is approximately given by

$$S_m(T=0) = \frac{16Z^2e^4}{3\hbar M\omega_0^3 b^4}, \tag{14}$$

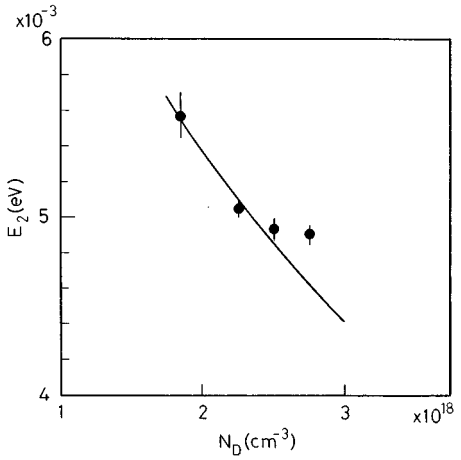

FIG. 13. The donor concentration dependence of the ionization energy E_2. The solid curve represents Eq. (15).

where $+Z$ $(-Z)$ is the charge of a positive (negative) lattice ion, M is the reduced ion mass, and b is the lattice distance.[16] It follows that $m^{**}\cong(1.3-5.0)m^*\cong(4-25)m_e$ for $\omega_0=1.5\times10^{14}$ s^{-1}, $m^*\cong(3-5)m_e$ and $b=2.96$–4.6 Å. These values, which are calculated by neglecting the anisotropy in both large and small polaron models, are of the same order of magnitude as those obtained in the present experiments.

B. Ionization energy of a donor center

Between about 4 and 20 K, both ρ and R_H decrease with increasing temperature, and the carrier concentration n increases with increasing temperature according to Eq. (1). In addition, resistivity decreases with increasing O_d. Upon doping of Al, which acts as an acceptor, resistivity increases due to the compensation effect.[5] These results indicate that the ionization of donor centers takes place in this temperature region. Our EPR experiments performed at 4.2 K revealed that, for $O_d<10^{19}$/cm^3, the main defects are C centers, which were assigned to be Ti interstitial ions, and which increase in number with increasing O_d.[9–11] EPR and channeling experiments[13] demonstrated that the dominant defects in the O_d region investigated in the present study are Ti interstitials. Therefore, the activation energy E_2 is an ionization energy for Ti interstitial donor centers. It exhibits O_d dependence (Fig. 4); for $O_d<1\times10^{19}$/cm^3 it decreases with increasing O_d, whereas for $O_d>1\times10^{19}$/cm^3 it increases with increasing O_d. In the case of p-type Si it has been reported that ionization energy decreases with increasing acceptor concentration N_A in the form of $E_0-\gamma N_A^{1/3}$ (Ref. 35). If we assume that E_2 here has a similar dependence upon donor concentration N_D $(\cong\frac{1}{2}O_d)$, it can be approximated by

$$E_2=0.0121-5.33\times10^{-9}N_D^{1/3}\ \text{(eV)}, \tag{15}$$

in the region $O_d<5.5\times10^{18}$/cm^3, although the concentration range investigated in the present study is very narrow compared with the case of Si (Fig. 13). The ionization energy at the limit of low donor concentration, E_0, is about 0.012 eV. Taking account of the error bars of the data points, E_0 ranges from 0.0098 to 0.014 eV. In the case of the large polaron, Simpson[36] calculated the ionization energy E_2 of an electron trapped at an interstitial defect in an ionic crystal assuming a hydrogenlike wave function for the trapped electron, and found that E_2 can be approximated by $E_2\cong m^*e^4/(2\hbar^2\kappa_{st}^2)$ for small values of α and β where $\beta=e^2u/\kappa_{st}\hbar\omega_0$. When $\beta=1$, the region of α where this approximation can be applied extends up to 6. The smaller the value of β, the larger this region becomes. In the case of rutile, $\beta\cong0.35$–0.45 and $\alpha=2.7$–3.5, so the above relation can be applied. Using $m^*\cong(3-5)m_e$ and $\kappa_{st}\cong117$, we obtain $E_2\cong0.003$–0.005 eV. On the other hand, in the small polaron model, the donor ionization energy is of the order of $e^2/\kappa_{st}d$, where d is the distance between a donor center and the nearest Ti ion.[37] In the case of rutile, $e^2/\kappa_{st}d\cong0.05$ eV. The value $E_0=0.0098$–0.014 eV falls in the intermediate region between these two.

C. Two-band conduction

We discuss the small R_H maxima or shoulders around 110 K in terms of the two-conduction-band model proposed by Becker and Hosler.[3,8] At low temperatures the contribution of the lower band is predominant, while above about 80 K electrons become excited into the upper band and its contribution becomes larger with increasing temperature. The maxima or shoulders result from the difference in mobility between these two bands. In the following, the analysis will be performed for specimens $B1ca$ and $B1ac$ in which the defects are mostly Ti interstitial ions. According to the two-conduction-band model, $R_{H,a}$ and $R_{H,c}$ are given by

$$R_{H,a}=\frac{1}{ec}\,\frac{r_{la}MQDE+r_{ua}}{(MQD+1)(MQE+1)}\,\frac{MQ+1}{n},$$

$$R_{H,c}=\frac{1}{ec}\,\frac{r_{lc}MQD^2+r_{uc}}{(MQD+1)^2}\,\frac{MQ+1}{n}, \tag{16}$$

where the subscripts l and u denote the quantities associated with the lower and upper conduction bands, respectively.[8,20] In addition, n, MQ, D, and E are defined as

$$n_l/n_u=(m_{dl}^{**}/m_{du}^{**})^{3/2}\exp(\Delta E/kT)\equiv MQ,$$

$$n_l+n_u\equiv n, \tag{17}$$

$$D\equiv\mu_{la}/\mu_{ua},\quad E\equiv\mu_{lc}/\mu_{uc},$$

where ΔE is the energy separation between the upper and lower band minima. The quantities r_a and r_c are Hall factors given by $R_{H,a}=r_a/nec$ and $R_{H,c}=r_c/nec$. As noted in Sec. IV A, r_{la} and r_{lc} are taken equal to unity, i.e., $r_{la}=r_{lc}=1$.

The carrier concentration n can be calculated when $M^{2/3}=(m_{dl}^{**}/m_{du}^{**})$ and ΔE are known. For specimens $B1ac$ and $B1ca$, $E_2=0.0055$ eV and $N_D=3.7\times10^{18}$/cm^3. Using $m_{dl}^{**}=7m_e$, the acceptor concentration is estimated from Eq. (1) to be $N_A=1.63\times10^{18}$/cm^3. The Hall coefficients $R_{H,a}$ and $R_{H,c}$ were calculated for various sets of parameters $(\Delta E,m_{dl}^{**}/m_{du}^{**},D,E,r_{ua},r_{uc})$ under the assumption that they are temperature independent. An energy separation ΔE in the range of 0.03–0.05 eV gives good agreement between experimental and calculated $R_{H,a}$ and $R_{H,c}$ curves. Fairly good agreement was obtained for the sets of parameters (0.047 eV, 10, 0.0001, 0.00079, 0.0023, 0.0019) and (0.047

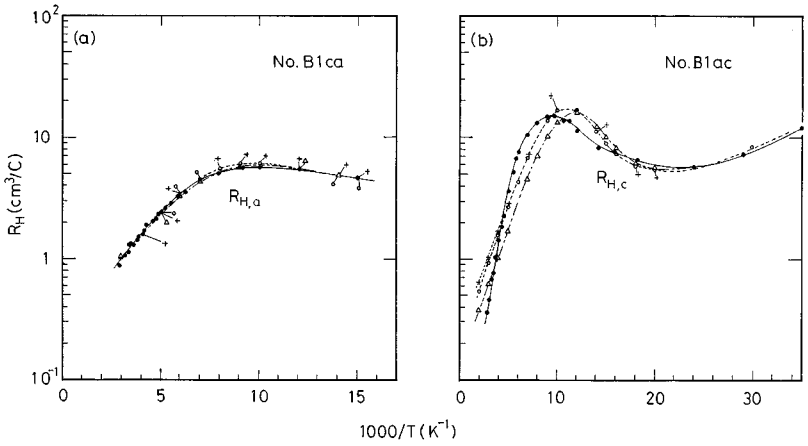

FIG. 14. Comparison of experimental and calculated values of Hall coefficients for specimens (a) $B1ca$ ($R_{H,a}$) and (b) $B1ac$ ($R_{H,c}$). Solid curves represent the experimental results. Calculated results were obtained for three sets of parameters, ($\Delta E, m_{dl}^{**}/m_{du}^{**}, D, E, r_{ua}, r_{uc}$): ○ for (0.047 eV, 10, 0.0001, 0.00079, 0.0023, 0.0019), △ for (0.047 eV, 1.7, 0.001, 0.013, 0.033, 0.017), and + for (0.047 eV, 1.7, 0.0015, 0.011, 0.032, 0.029).

eV, 1.7, 0.0015, 0.011, 0.032, 0.029), but these parameters cannot be determined uniquely. The calculated results are shown in Fig. 14. They give better agreement in the case of $R_{H,a}$ than $R_{H,c}$, and are more sensitive to the values of r_{ua} and r_{uc} than to those of D and E. The difference between calculated and experimental values results partly from neglecting the temperature dependence of M, D, E, r_{ua}, and r_{uc}. Becker and Hosler[8] obtained 0.04–0.06 eV for ΔE from the analysis of anisotropy ratios of Hall coefficients. By a similar analysis, $\Delta E = 0.023$ eV was obtained from the present data. The maximum on the $R_{H,a}$ curve is not as large as that on the $R_{H,c}$ curve because the difference in mobility between the lower and upper bands is smaller in the **c** direction than in the **a** direction.

The smallness of values of r_{ua} and r_{uc} suggests that the upper conduction band is rather anisotropic as pointed out by Becker and Hosler[8] and Herring.[38] The conduction bands of rutile originate from the $3d$ level of Ti ions. The calculation by Kahn and Leyendecker[39] suggests the splitting of the conduction band due to the orthorhombic environment of Ti by the order of several hundredths of an eV. The analysis above indicates that the donor centers are mostly exhausted at about 250 K. As an example, the calculated temperature dependence of carrier concentrations n_l and n_u for $m_{dl}^{**}/m_{du}^{**} = 1.7$ is shown in Fig. 15. Therefore, the temperature dependence of R_H curves above 250 K is determined only through that of the MQ values. This is the reason why E_3 is independent of the oxygen deficiency O_d.

From the discussion above the small R_H maximum or shoulder around 110 K is explained qualitatively based on the two-conduction-band model. The energy separation between the bottom of the lower conduction band and the bottom of the upper one is 0.03–0.05 eV, and the mobility of an upper-band electron is higher than that of a lower-band electron.

D. Mobility above 50 K

Above about 30 K, the mobility becomes weakly dependent on O_d and decreases rapidly with increasing temperature (Fig. 5). In this temperature region phonon scattering becomes dominant. For example, from 30 to 100 K the carrier concentration increases gradually by a factor of about 2.5 (Fig. 15), while the mobility greatly decreases by a factor of more than 10. Therefore, the observed increase of ρ with increasing temperature above 30 K is attributed to the decrease of mobility. According to the two-conduction-band model, the contribution of the upper-band electrons having

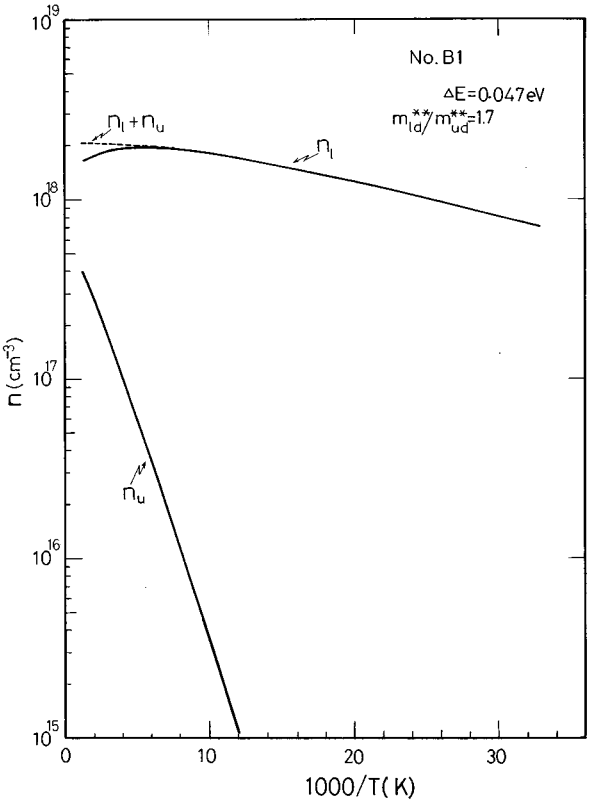

FIG. 15. Carrier concentrations in the upper and lower conduction bands n_u and n_l of specimen $B1ca$ estimated using the two-conduction-band model for $\Delta E = 0.047$ eV and $m_{dl}^{**}/m_{du}^{**} = 1.7$.

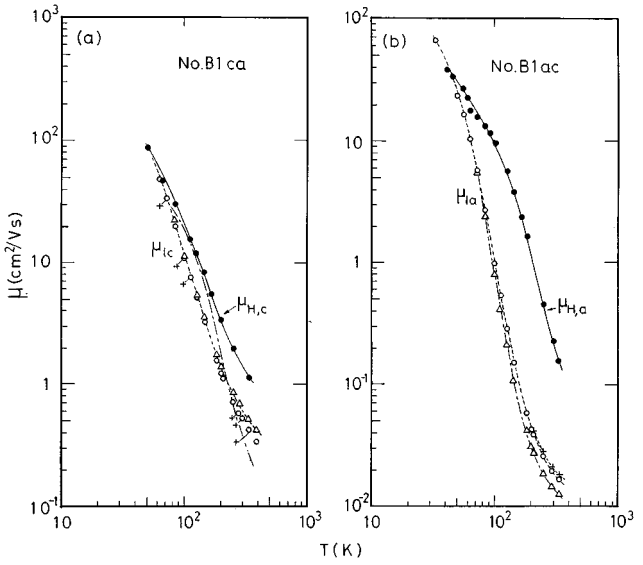

FIG. 16. (a) Hall mobilities $\mu_{H,c}(=R_{H,a}/\rho_c)$ and drift mobilities μ_{lc} of the lower-conduction-band electrons estimated using the two-conduction-band model for specimen $B1ca$ for three sets of parameters, $(\Delta E, m_{dl}^{**}/m_{du}^{**}, D, E)$: ○: (0.047 eV, 10, 0.0001, 0.00079); △: (0.047 eV, 1.7, 0.001, 0.013); and +: (0.047 eV, 1.7, 0.0015, 0.011). The mobilities given by Eq. (20) and the mobilities calculated using Eq. (22) for $m^*=4m_e$ and $\langle m^{**}\rangle=72m_e$ are indicated by a dotted curve and a chain curve, respectively. (b) Hall mobilities $\mu_{H,a}(=R_{H,c}/\rho_a)$ and drift mobilities μ_{la} of the lower-conduction-band electrons estimated for specimen $B1ac$ in the same way as for specimen $B1ca$ and using the same three sets of parameters $(\Delta E, m_{dl}^{**}/m_{du}^{**}, D, E)$. The curves were drawn only to guide the eye.

higher mobility becomes large above about 100 K. For specimen $B1ca$ the temperature dependence of the mobility in the **c** direction above 50 K of the lower-band electrons, $\mu_{l,c}$, was estimated from the electrical conductivity data under the assumption that M, D, E, and r_{ua} are temperature independent. The results are shown in Fig. 16(a). Taking account of the contributions of both optical and acoustic-phonon scattering, the mobility μ is given by

$$\frac{1}{\mu}=\frac{1}{\mu_{\rm opt}}+\frac{1}{\mu_{\rm acoust}}. \tag{18}$$

In the large polaron model, the drift mobility $\mu_{\rm opt}$ is given by the following equation in the temperature region where $\hbar\omega_0/kT\gg1$:[40]

$$\mu_{\rm opt}=\frac{e}{2m^*\alpha\omega_0}\left(\frac{m^*}{m^{**}}\right)^3 f(\alpha)\exp(\hbar\omega_0/kT),\quad f(\alpha)\cong1. \tag{19}$$

For the acoustic-phonon scattering, $\mu_{\rm acoust}\propto T^{-3/2}$. The μ_{lc} values estimated above can be approximated by the equation

$$\frac{1}{\mu_{lc}}=8.49\ \exp(-534/T)+4.47\times10^{-5}T^{3/2}\ \ ({\rm cm}^{-2}\ {\rm V\ s}), \tag{20}$$

as indicated by a dotted curve in Fig. 16(a). The longitudinal optical phonon has three modes with $\omega_0=7.0\times10^{13}$, 8.7×10^{13}, and 1.5×10^{14} s^{-1} (Ref. 15). Equation (20) seems to indicate that the interaction with the mode with $\omega_0=7.0\times10^{13}$ s^{-1} ($\hbar\omega_0/k\cong534$ K) is the most effective in this temperature region. Assuming $m^{**}=(1+\alpha/6)m^*$ and $f(\alpha)=1$, the values of m^{**} and m^* can be estimated from Eqs. (19) and (20) as a function of α; for $\alpha=1$, $m^{**}\cong78m_e$, and $m^*\cong67m_e$, for $\alpha=2$, $m^{**}\cong30m_e$, and $m^*\cong23m_e$, and for $\alpha=5$, $m^{**}\cong6.3m_e$, and $m^*\cong3.5m_e$. According to the estimation by Eagle,[15] the coupling constant α for the mode with $\omega_0=7.0\times10^{13}$ s^{-1} is the smallest among the three modes and is given by $\alpha=0.05(m^*/m_e)^{1/2}$. The α and m^* values estimated above, however, do not satisfy this relation. If all three modes are taken into account, the mobility $\mu_{\rm opt}$ may be obtained from the formula $\mu_{\rm opt}=e\tau_{\rm opt}/\langle m^{**}\rangle$ with an average effective mass $\langle m^{**}\rangle$ and a relaxation time $\tau_{\rm opt}$, which is given by

$$\frac{1}{\tau_{\rm opt}}=\sum_{j=1}^{3}\left(\frac{1}{\tau_{{\rm opt},j}}\right)=\sum_{j=1}^{3}\left(\frac{e}{m_j^{**}\mu_{{\rm opt},j}}\right), \tag{21}$$

where each $\tau_{{\rm opt},j}$ is a relaxation time associated with an individual mode j.[15] The mobility can, therefore, be expressed by

$$\frac{1}{\mu}=\frac{A_1}{\tau_{\rm opt}}+A_2T^{3/2}, \tag{22}$$

and the average effective mass can be estimated from the value of A_1. Using α_j values estimated by Eagle,[15] the relation $m^{**}=(1+\alpha/6)m^*$ and Eq. (19) for each individual mode, and Eq. (21), the coefficients A_1 and A_2 were determined so that the mobilities given by Eq. (22) would take values as close as possible to μ_{lc} for various values of m^* between m_e and $10m_e$. The average effective mass was estimated from the values of A_1 to be $\langle m^{**}\rangle>31m_e$. As an example, mobilities thus calculated for $m^*=4m_e$ and $\langle m^{**}\rangle=72m_e$ are shown in Fig. 16(a) as a chain curve. The fit of μ_{lc} to Eq. (22) is not very good and the estimated $\langle m^{**}\rangle$ is also much larger than that derived in Sec. IV A. There remains some uncertainty in the estimation of μ_{lc} and in the fitting to Eqs. (20) and (22) due to the following two assumptions: (1) In deriving μ_{lc} the parameters M, D, E, and r_{ua} were assumed to be temperature independent, and (2) in the fitting to Eqs. (20) and (22) the anisotropy in effective mass was neglected as a result of the use of Eq. (19). However, it seems to be difficult to explain the mobility above 50 K of the lower-band electrons in terms of the large polaron intermediate coupling model.

The conductivity in the **a** direction σ_a increases with increasing-temperature above 250 K, while this is not the case for σ_c (Figs. 6 and 7). Such an increase in σ_a was also observed by Bogomolov and Zhuze, while in the **c** direction it was not observed up to 600 K, or at least not so conspicuously as in the **a** direction.[41] The drift mobility in the **a** direction μ_{la} can be estimated in a similar way to that for μ_{lc}. The estimated mobilities μ_{la} for specimen $B'1ac$ are shown in Fig. 16(b). μ_{la} has smaller values than μ_{lc} and a different temperature dependence. It is probable that in an anisotropic crystal the mobility has different temperature dependences for different directions. The decrease of μ_{la} with increasing temperature becomes slower above 250 K. When

the conductivity continues to increase at higher temperatures, as observed by Bogomolov and Zhuze,[41] μ_{la} increases with temperature; the increase in conductivity with temperature is attributed to the increase in mobility. This is characteristic of the hopping conduction mediated by small polarons.[14] These results suggest that the small polaron model is appropriate for the discussion of conduction by lower band electrons, at least, in the **a** direction, though there is some uncertainty in the estimation of μ_{la} because the $R_{H,c}$ curve was fitted assuming M, D, E, and r_{uc} to be temperature independent, and rather less successfully than the $R_{H,a}$ curve.

V. SUMMARY

Based on electrical resistivity ρ and Hall coefficient R_H measurements from 2 to 370 K on slightly reduced semiconductive rutile single crystals with various oxygen deficiencies O_d from 3.7×10^{18} to $1.3\times10^{19}/cm^3$, electronic conduction above 4 K was discussed. According to the results of our EPR and channeling experiments, defects are mostly Ti interstitial ions in this range of O_d.

Ionization of Ti interstitial donors takes place above about 4 K. The ionization energy E_2 depends on the donor concentration N_D. If E_2 has an N_D dependence given by $E_2=E_0-\gamma N_D^{1/3}$ as in the case of Si, it can be approximated with $E_0=0.012\pm0.002$ eV for $O_d<5.5\times10^{18}/cm^3$, although the range of N_D investigated in the present experiment is narrow.

On the R_H curves a small maximum or shoulder is observed around 110 K. This is interpreted in terms of two conduction bands, which are separated by 0.03–0.05 eV in energy at the bottom of the band. The upper-band electron has a smaller effective mass, larger mobility, and larger anisotropy than the lower-band electron. The contribution of the upper band to the electronic conduction becomes conspicuous above about 100 K.

From the R_H data below 20 K the density of states effective mass m_d^{**} of the lower conduction band was estimated to be about $(7–8)m_e$. The anisotropy of the effective mass was roughly estimated to be $m_c^{**}\cong(2–4)m_e$ and $m_a^{**}\cong(10–16)m_e$ from measurements of mobility and the anisotropy in resistivity.

The mobility above 50 K of the lower conduction-band electrons was also discussed. For this temperature range, at least in the **a** direction, the small polaron model must be taken into account.

ACKNOWLEGMENTS

The authors thank Professor T. Sugawara for his support in the low-temperature experiments at the early stage of this research and S. Takahashi for his help in the specimen preparation. The authors also thank R. Macrae for his suggestion in the preparation of this manuscript.

[1] F. A. Grant, Rev. Mod. Phys. **31**, 646 (1959).
[2] R. R. Hasiguti, K. Minami, and H. Yonemitsu, J. Phys. Soc. Jpn. **16**, 2223 (1961).
[3] H. Becker and W. R. Hosler, Proceedings of the International Conference on Crystal Lattice Defects, Tokyo and Kyoto, 1962 [J. Phys. Soc. Jpn. Suppl. II **18**, 152 (1963)].
[4] R. R. Hasiguti, N. Kawamiya, and E. Yagi, *Proceedings of the 7th International Conference on the Physics of Semiconductors, Paris, 1964* (Dunod, Paris, 1965), p. 1225.
[5] R. R. Hasiguti and E. Yagi, Phys. Rev. B **49**, 7251 (1994).
[6] V. N. Bogomolov, E. K. Kudinov, and Yu, A. Firsov, Fiz. Tverd Tela **9**, 3175 (1967) [Sov. Phys. Solid State **9**, 2502 (1968)].
[7] G. A. Acket and J. Volger, Physica **32**, 1680 (1966).
[8] J. A. Becker and W. R. Hosler, Phys. Rev. **137**, A1872 (1965).
[9] R. R. Hasiguti, E. Iguchi, and S. Takahashi, in *Proceedings of the 9th International Conference on the Physics of Semiconductors, Moscow, 1968* (Nauka, Leningrad, 1968), p. 1142.
[10] R. R. Hasiguti, Annu. Rev. Mater. Sci. **2**, 69 (1972).
[11] M. Aono and R. R. Hasiguti, Phys. Rev. B **48**, 12 406 (1993).
[12] E. Yagi and R. R. Hasiguti, J. Phys. Soc. Jpn. **43**, 1998 (1977); *Lattice Defects in Semiconductors* (Institute of Physics, London, 1974), p. 359.
[13] E. Yagi, A. Koyama, H. Sakairi, and R. R. Hasiguti, J. Phys. Soc. Jpn. **42**, 939 (1977).
[14] J. Appel, *Solid State Physics*, edited by F. Seitz, D. Turnbull, and H. Ehrenreich (Academic, New York, 1968), p. 193.
[15] P. M. Eagle, J. Phys. Chem. Solids **25**, 1243 (1964).
[16] G. L. Sewell, Philos. Mag. **3**, 1361 (1958).
[17] L. Friedman, Phys. Rev. **131**, 2445 (1963).
[18] T. H. Geball, *Semiconductors*, edited by N. B. Hannay (Reinhold Publishing, New York, 1959), p. 330.
[19] G. L. Bir, V. N. Bogomolov, E. V. Krivitskii, and T. E. Sulyatitskaya, Fiz. Tverd Tela **7**, 2978 (1965) [Sov. Phys. Solid State **7**, 2414 (1966)].
[20] W. C. Hernandez, Jr. and A. H. Kahn, J. Res. NBS **67**A, 293 (1963).
[21] A. G. Samoilovich, I. Ya. Korenblit, and I. V. Dakhovskii, Dokl. Akad. Nauk SSSR **139**, 355 (1961) [Sov. Phys. Dokl. **6**, 606 (1962)].
[22] A. G. Samoilovich, I. Ya. Korenblit, I. V. Dakhovskii, and V. D. Iskra, Fiz. Tverd, Tela (Leningrad) **3**, 3285 (1961) [Sov. Phys. Solid State **3**, 2385 (1962)].
[23] I. Ya. Korenblit, Fiz. Tverd, Tela (Leningrad) **4**, 166 (1962) [Sov. Phys. Solid State **4**, 1225 (1962)].
[24] W. Schmidt, Ann. Phys. (Leipzig) **9**, 919 (1902); **11**, 114 (1903).
[25] W. R. Thurber and A. J. H. Mante, Phys. Rev. **139**, 1655 (1962).
[26] V. Cristea and V. Babes, Phys. Status Solid, A **45**, 617 (1978).
[27] H. P. R. Frederikse, J. Appl. Phys. **32**, 2211 (1961).
[28] J. F. Baumard and F. Gevais, Phys. Rev. B **15**, 2316 (1977).
[29] J. Pascual, J. Camassel, and H. Mathieu, Phys. Rev. B **18**, 5606 (1978).
[30] T. R. Sandin and P. H. Keeson, Phys. Rev. **177**, 1370 (1969).
[31] J. W. DeFord and O. W. Johnson, J. Appl. Phys. **54**, 889 (1983).
[32] H. Fröhlich, H. Pelzer, and S. Zienau, Philos. Mag. **41**, 221 (1950).
[33] T. D. Lee, F. E. Low, and D. Pines, Phys. Rev. **90**, 297 (1953).
[34] T. D. Schultz, Phys. Rev. **116**, 526 (1959).
[35] G. L. Pearson and J. Bardeen, Phys. Rev. **75**, 865 (1949).

[36] J. H. Simpson, Proc. R. Soc. London A **231**, 308 (1955).
[37] N. F. Mott, Comments Solid State Phys. **1**, 105 (1968).
[38] C. Herring, Bell Syst. Tech. J. **34**, 237 (1955).
[39] A. H. Kahn and A. J. Leyendecker, Phys. Rev. **135**, A1321 (1964).
[40] F. E. Low and D. Pines, Phys. Rev. **98**, 414 (1955).
[41] V. N. Bogomolov and V. P. Zhuze, Fiz. Tverd Tela **5**, 3285 (1963) [Sov. Phys. Solid State **5**, 2404 (1964)].